2016

TREM2-mediated early microglial response limits diffusion and toxicity of amyloid plaques

Yaming Wang
Washington University School of Medicine in St. Louis

Tyler K. Ulland
Washington University School of Medicine in St. Louis

Jason D. Ulrich
Washington University School of Medicine in St. Louis

Wilbur Song
Washington University School of Medicine in St. Louis

Thomas E. Mahan
Washington University School of Medicine in St. Louis

See next page for additional authors

TREM2-mediated early microglial response limits diffusion and toxicity of amyloid plaques

Yaming Wang,[1,5]* Tyler K. Ulland,[1]* Jason D. Ulrich,[2,3,4]* Wilbur Song,[1] John A. Tzaferis,[5] Justin T. Hole,[5] Peng Yuan,[6] Thomas E. Mahan,[2,3,4] Yang Shi,[2,3,4] Susan Gilfillan,[1] Marina Cella,[1] Jaime Grutzendler,[6] Ronald B. DeMattos,[5] John R. Cirrito,[2,3,4] David M. Holtzman,[2,3,4] and Marco Colonna[1]

[1]Department of Pathology and Immunology, [2]Department of Neurology, [3]Knight Alzheimer's Disease Research Center, and [4]Hope Center for Neurological Disorders, Washington University School of Medicine, St. Louis, MO 63110
[5]Eli Lilly and Company, Lilly Corporate Center, Indianapolis, IN 46285
[6]Department of Neurology, Yale University, New Haven, CT 06520

Triggering receptor expressed on myeloid cells 2 (TREM2) is a microglial receptor that recognizes changes in the lipid microenvironment, which may occur during amyloid β (Aβ) accumulation and neuronal degeneration in Alzheimer's disease (AD). Rare *TREM2* variants that affect TREM2 function lead to an increased risk of developing AD. In murine models of AD, TREM2 deficiency prevents microglial clustering around Aβ deposits. However, the origin of myeloid cells surrounding amyloid and the impact of TREM2 on Aβ accumulation are a matter of debate. Using parabiosis, we found that amyloid-associated myeloid cells derive from brain-resident microglia rather than from recruitment of peripheral blood monocytes. To determine the impact of TREM2 deficiency on Aβ accumulation, we examined Aβ plaques in the 5XFAD model of AD at the onset of Aβ-related pathology. At this early time point, Aβ accumulation was similar in TREM2-deficient and -sufficient 5XFAD mice. However, in the absence of TREM2, Aβ plaques were not fully enclosed by microglia; they were more diffuse, less dense, and were associated with significantly greater neuritic damage. Thus, TREM2 protects from AD by enabling microglia to surround and alter Aβ plaque structure, thereby limiting neuritic damage.

Alzheimer's disease (AD) is the most common form of late-onset dementia. Key pathological features of AD consist of the deposition of amyloid-β peptide (Aβ) and hyperphosphorylated tau aggregates that, together, are linked with synapse loss and neuronal cell death, as well as activation of microglia and astrocytes (Holtzman et al., 2011). Rare forms of autosomal dominant inherited AD are caused by mutations in genes involved in the Aβ processing pathway, such as amyloid precursor protein (*APP*) and presenilin 1 (*PSEN1*; Tanzi, 2012). The origin of nonfamilial AD is less well understood and may depend on a combination of genetic and nongenetic risk factors (Tanzi, 2012). Recent genome-wide association studies have identified rare variants of genes that encode immune receptors as risk factors (Guerreiro and Hardy, 2014; Karch and Goate, 2015). Among these, the arginine 47 histidine (R47H) variant of triggering receptor expressed on myeloid cells 2 (TREM2) has been found in several cohorts of patients. TREM2 is a cell surface receptor of the Ig superfamily that is expressed in microglia of the central nervous system and in other tissue macrophages, and binds phospholipids and other polyanionic ligands (Paloneva et al., 2002; Daws et al., 2003; Cannon et al., 2012; Wang et al., 2015). TREM2 transmits intracellular signals through the associated adaptor DNAX activation protein of 12 kD (DAP12), which recruits the protein tyrosine kinase spleen tyrosine kinase. TREM2 signaling promotes survival, proliferation, phagocytosis, and secretion of cytokines and chemokines (Takahashi et al., 2005; Otero et al., 2009; Wang et al., 2015). TREM2-induced signals also augment activation of integrins, thereby facilitating adhesion and remodeling of the actin cytoskeleton (Takahashi et al., 2005).

We and others have recently examined the impact of TREM2 deficiency on the microglial response to Aβ deposition in mouse models of AD, including APPPS1-21 and 5XFAD mice (Ulrich et al., 2014; Jay et al., 2015; Wang et al., 2015). All studies showed that TREM2 deficiency affects clustering of microglia around the plaques. However, whether Aβ-reactive microgliosis involves resident microglia (Wang et al., 2015) or myeloid cells derived from peripheral blood monocytes (Jay et al., 2015) is still up for debate. Additionally, the analysis of Aβ accumulation in different mouse models of AD yielded inconsistent results

*Y. Wang, T.K. Ulland, and J.D. Ulrich contributed equally to this paper.

Correspondence to Marco Colonna: mcolonna@pathology.wustl.edu; or David M. Holtzman: holtzman@neuro.wustl.edu

Abbreviations used: Aβ, amyloid β; AD, Alzheimer's disease; APP, amyloid precursor protein; BBB, blood–brain barrier; PS1, Presenilin 1; TREM2, triggering receptor expressed on myeloid cells 2.

The Rockefeller University Press $30.00
J. Exp. Med. 2016 Vol. 213 No. 5 667–675
www.jem.org/cgi/doi/10.1084/jem.20151948

(Tanzi, 2015). In 8-mo-old 5XFAD mice, TREM2 deficiency resulted in increased hippocampal Aβ accumulation, consistent with a protective function of TREM2 (Wang et al., 2015). In 4-mo-old APPPS1-21 mice lacking TREM2, however, hippocampal Aβ accumulation was paradoxically reduced despite the myeloid cell defect, a finding that was interpreted to indicate that TREM2 deficiency protects against AD pathogenesis (Jay et al., 2015).

In this study, we determined whether the Aβ-reactive myeloid cells are derived from resident microglia or from infiltrating monocytes in parabiosis experiments. Using this approach, we observed no infiltration of monocytes around Aβ plaques in either 5XFAD or APPPS1-21 mice. Moreover, staining of brain sections for the proliferation marker Ki67 revealed that TREM2 is necessary for local proliferation of microglia around the plaques. To explain the conflicting results regarding the impact of TREM2 deficiency on Aβ accumulation, we hypothesized that whereas TREM2 deficiency results in early impairment of the microglial response to Aβ deposits in all AD models, changes in Aβ burden develop more slowly; therefore, the discrepancies in Aβ accumulation may be a result of the varied timing of the analyses—8 mo in 5XFAD mice (Wang et al., 2015) and 3–4 mo in APPPS1-21 mice (Ulrich et al., 2014; Jay et al., 2015). To test this, we examined microgliosis and Aβ deposition at early time points (4 mo) in TREM2-deficient and -sufficient 5XFAD mice. We found that Aβ deposition was quantitatively similar in the presence and absence of TREM2. However, TREM2 did affect microglial clustering and the structure of Aβ plaques at this early time point; in 5XFAD mice lacking TREM2, Aβ plaques appeared more diffuse, had altered Aβ subspecies composition, and were associated with increased neuritic dystrophy compared with those in TREM2-sufficient 5XFAD mice. Collectively, our data demonstrate that TREM2 is required for the early expansion of microglia around Aβ plaques that limits plaque diffusion as well as amyloid-related neuronal damage.

RESULTS AND DISCUSSION

Aβ-reactive myeloid cells derive from brain-resident microglia

It has been proposed that the TREM2-dependent microglial response to Aβ plaques in APPPS1-21 mice relies on the recruitment of blood monocytes (Jay et al., 2015). We first determined whether blood monocytes in 5XFAD mice express TREM2 and hence might respond to putative TREM2 ligands present in peripheral blood during Aβ accumulation. Staining of monocytes from 5XFAD and wild-type mice with anti-TREM2 revealed no detectable expression of TREM2 (Fig. 1 A). However, it remained possible that monocytes up-regulate TREM2 upon infiltrating the brain and, therefore, TREM2 would be required for clustering of infiltrating monocyte around Aβ plaques. To definitively test for contribution of blood monocytes to the microglial pool in 5XFAD mice, we performed parabiosis experiments in which the blood circulation of CD45.2$^+$ 5XFAD mice was joined with that of age-matched congenic CD45.1$^+$ B6 mice (Fig. 1, B–E). Parabiosis was performed in 4-mo-old mice or in 8-mo-old mice. After 4 weeks, tissues were analyzed. Total blood leukocytes and lung alveolar macrophages showed a marked degree of exchange (Fig. 1, B and C). In contrast, nearly all microglia in 5XFAD and B6 mice maintained expression of the original CD45.2 or CD45.1 marker, respectively, consistent with minimal monocyte infiltration (Fig. 1, B–E). Upon expanding this analysis to APPPS1-21 mice we found results consistent with a lack of infiltration of CD45.1$^+$ cells into the brain of CD45.2$^+$ APPPS1-21 mice (Fig. 1, F and G). Thus, the contribution of peripheral monocytes to the microglial pool in both 5XFAD and APPPS1-21 models of AD is negligible.

TREM2 deficiency affects plaque-associated microglial proliferation

We previously observed an impaired microglial response to Aβ in 8-mo-old *Trem2*$^{-/-}$ 5XFAD mice (Wang et al., 2015). Defective microglial clustering around plaques was also detected at earlier time points in 3- or 4-mo-old *Trem2*$^{-/-}$ APPPS1-21 mice (Ulrich et al., 2014; Jay et al., 2015). To test whether *Trem2*$^{-/-}$ 5XFAD mice also had an early microglial defect, we compared the total number of microglia in 4- and 8-mo-old 5XFAD and *Trem2*$^{-/-}$ 5XFAD mice. Microglial numbers were similar in 4-mo-old 5XFAD and *Trem2*$^{-/-}$ 5XFAD mice. In contrast, at 8 mo of age, 5XFAD mice had a clear increase in total microglia, whereas age-matched *Trem2*$^{-/-}$ 5XFAD had fewer microglia (Fig. 2 A). We next assessed the number of plaque-associated microglia in 4-mo-old 5XFAD, *Trem2*$^{+/-}$ 5XFAD, and *Trem2*$^{-/-}$ 5XFAD mice. 5XFAD mice had significantly more microglial clustering around plaques than did *Trem2*$^{+/-}$ and *Trem2*$^{-/-}$ 5XFAD mice (Fig. 2, B and C). Thus, an impairment of microglial response to Aβ deposits was detectable even at 4 mo of age in *Trem2*$^{-/-}$ 5XFAD mice.

Given that brain-resident microglia are capable of self-renewal and expansion (Gomez Perdiguero et al., 2013; Greter and Merad, 2013; Prinz and Priller, 2014), we next sought to determine if microglia associated with plaques resulted from the proliferation of resident microglia. We analyzed nuclear localization of Ki-67, a well-characterized proliferation marker, in microglia from 4-mo-old 5XFAD and *Trem2*$^{-/-}$ 5XFAD mice in relation to their proximity to a plaque (Fig. 2, D–G). In 5XFAD mice, the majority of Ki-67$^+$ microglia detected were in close proximity to Aβ plaques (mean distance = 21.1 µm; Fig. 2, D and E). In contrast, plaque-associated Ki-67$^+$ microglia were nearly undetectable in *Trem2*$^{-/-}$ 5XFAD mice (Fig. 2 F). Additionally, we observed that Ki-67$^+$ microglia in 5XFAD mice were preferentially located near plaques with a greater volume (Fig. 2 G). As more proliferating microglia were

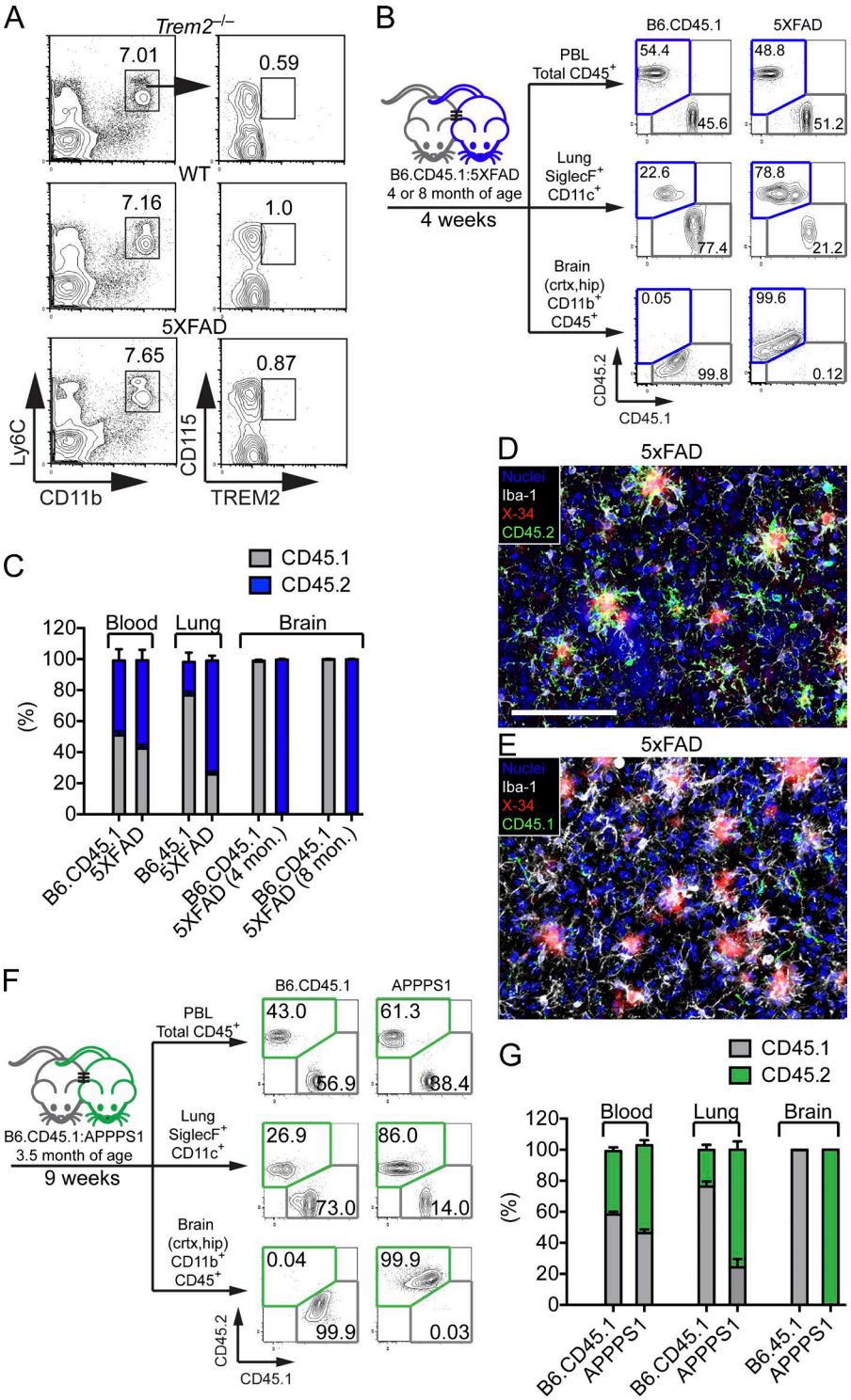

Figure 1. **Lack of monocyte contribution to amyloid-associated microglia.** (A) Surface expression of TREM2 among Ly6C$^+$ CD11b$^+$CD115$^+$ blood monocytes in WT and 5XFAD mice. *Trem2*$^{-/-}$ mice were used as negative controls. (B–E) Parabiosis was performed by joining blood circulation of 4- or 8-mo-old 5XFAD with age matched B6.CD45.1 congenic mice for 4 wk. (B) CD45$^+$ blood leukocytes, CD11c$^+$SiglecF$^+$ lung alveolar macrophages, and brain CD11b$^+$F4/80$^+$ microglia from parabionts were analyzed by flow cytometry. (C) Frequencies of CD45.1$^+$ and CD45.2$^+$ cells were compared in parabiotic partners. (D and E) Representative images of brain sections of an 8-mo-old 5XFAD parabiont stained with X-34 (red) for Aβ plaques and Iba-1 (white) for microglia. Contribution of host- and donor-derived microglia was examined using antibodies specific for CD45.2 (green; D) and CD45.1 (green; E). Nuclei were visualized with To-pro3 (blue). Bar, 100 µm (F and G) Parabiosis was performed using APPPS1-21 mice and age-matched B6.CD45.1 congenic mice for 9 wk. Parabionts were analyzed as described above. Data represent a total of five to seven mice per group in A–E and four mice per group in F and G.

observed near larger plaques in 5XFAD mice, we sought to determine if there was a correlation between the size of a plaque and the number of microglia associated with it. We found that, in 5XFAD mice, the number of microglia associated with a given plaque was positively correlated to the size of the plaque (Fig. 2 H). This correlation was not as strong in *Trem2*$^{+/-}$ 5XFAD and not apparent in *Trem2*$^{-/-}$ 5XFAD (Fig. 2 H).

Finally, as microglia are phagocytic and have been demonstrated to engulf pieces of plaques, we wished to examine the number of microglia which had internalized portions of plaques in 5XFAD and *Trem2*$^{-/-}$ 5XFAD

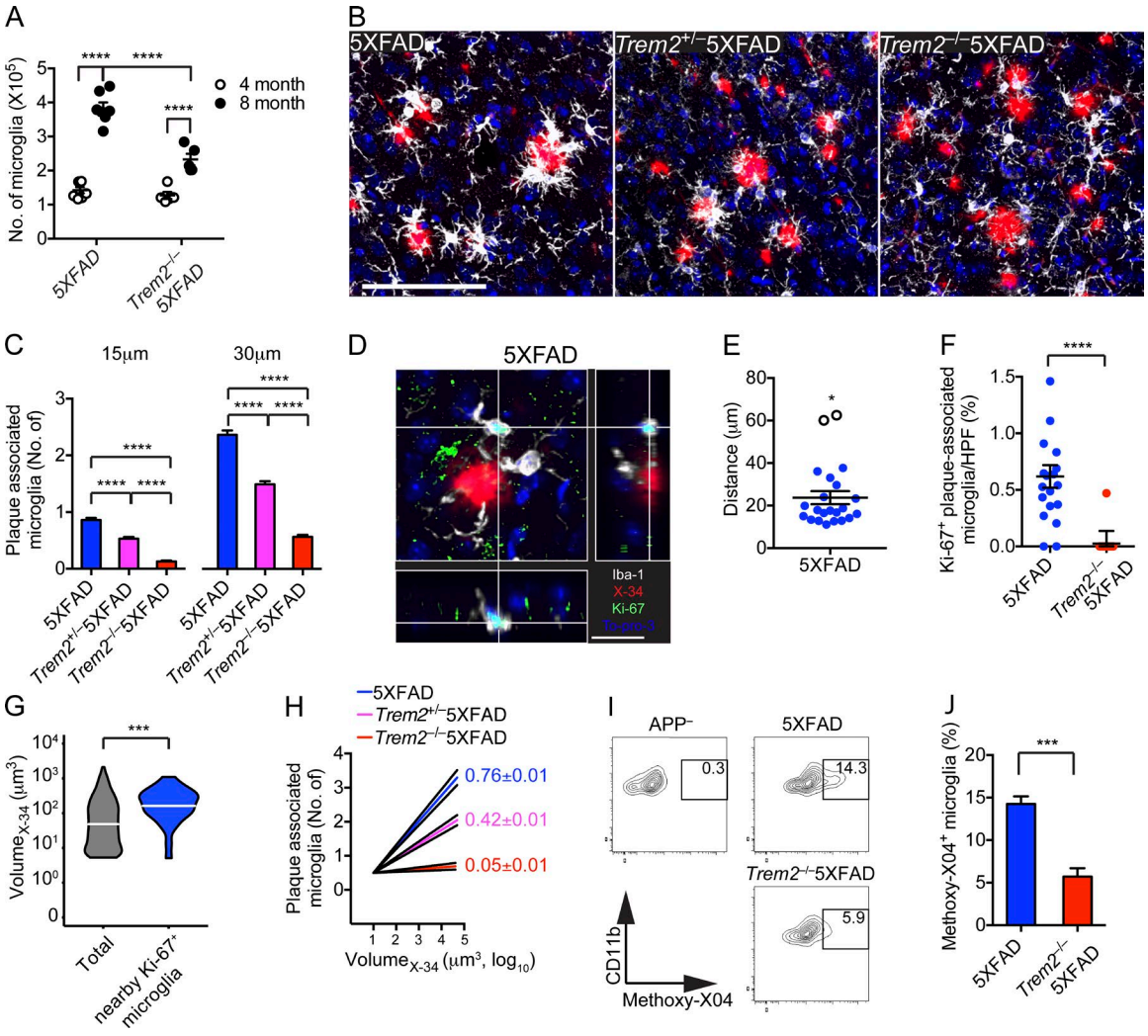

Figure 2. **Impaired microglial response to Aβ deposits in *Trem2*$^{-/-}$ 5XFAD mice is apparent by 4 mo.** (A) Total numbers of microglia in the cortices and hippocampi of 5XFAD and *Trem2*$^{-/-}$ 5XFAD mice at 4 and 8 mo of age. (B and C) Microglial response to Aβ plaques in 4-mo-ol 5XFAD, *Trem2*$^{+/-}$ 5XFAD, and *Trem2*$^{-/-}$5XFAD mice. (B) Representative images show matching cortical regions stained with X-34 (red) for amyloid plaques and Iba-1 (white) for microglia. Nuclei were visualized with To-pro3 (blue). (C) Numbers of microglia within 15 or 30 µm of Aβ plaques. (D–F) Microglia proliferation in 5XFAD and *Trem2*$^{-/-}$ 5XFAD mice was assessed by determining nuclear localization of Ki-67. (D) Representative sectional view of a confocal image shows expression of Ki-67 (green), microglia (Iba-1; white), and nuclei (blue). The proximity of Ki-67$^+$ microglia to Aβ plaques (X-34, red), in cortices of 5XFAD mice is visualized. (E) Proximity of Ki-67$^+$ microglia to the nearest plaque in cortices of 5XFAD. Unfilled circles (*) represent outliers as determined by q-test. (F) Frequencies of Ki-67$^+$ microglia per HPF in 5XFAD and *Trem2*$^{-/-}$*5XFAD* mice. (G) The volume of all observed Aβ plaques and Aβ plaques with Ki-67$^+$ in close proximity were compared. (H) The $\log_{10}$-transformed volume of plaques was plotted against the number of microglia within 15 µm. Numbers represent slope ±95% confidence interval. (I and J) 5XFAD and *Trem2*$^{-/-}$ 5XFAD mice were injected with methoxy-X04 and the percentage of microglia with internalized methoxy-X04 (indicative of fibrillar Aβ) was determined by flow cytometry. (I) Representative plots show methoxy-x04 positivity of CD11b$^+$CD45^{lo} cells. APP transgene negative (APP$^-$) littermates were used as negative controls. (J) The frequency of methoxy-X04$^+$ microglia was quantified. Bars: (B) 100 µm; (D) 20 µm. Error bar represents mean ± SEM. *, $P < 0.05$; ***, $P < 0.001$; ****, $P < 0.0001$, Mann-Whitney (A, F, and J) and q-test (E). Data represent a total of five to seven mice per group (A–F). For confocal images, a total of four random HPF were analyzed per mouse.

mice by measuring uptake of methoxy-X04, which binds to fibrillar Aβ (Heneka et al., 2013). Microglia in *Trem2*$^{-/-}$ 5XFAD mice incorporated less methoxy-X04 than microglia from 5XFAD mice (Fig. 2, I and J), corroborating that TREM2 deficiency impairs productive interactions between microglia and plaques. Collectively, these data indicate that TREM2-dependent accrual of resident microglia is a process that initiates early in Aβ deposition and depends at least in part on local proliferation of microglia around growing Aβ plaques.

TREM2 deficiency alters the physical appearance and composition of Aβ plaques

To determine if TREM2 impacted Aβ deposition at 4 mo of age, we compared the total insoluble $A\beta_{1\text{-}42}$ and $A\beta_{1\text{-}40}$ from 5XFAD, *Trem2*$^{+/-}$ 5XFAD, and *Trem2*$^{-/-}$ 5XFAD mice in the hippocampus and cortex by ELISA. We found no differences in the total $A\beta_{1\text{-}42}$ or $A\beta_{1\text{-}40}$ present in any of the genotypes (Fig. 3, A–D). Consistent with these findings, we did not detect a significant difference in X-34 staining in the cortices of *Trem2*$^{-/-}$ 5XFAD mice (Fig. 3 E). However, TREM2 had a remarkable influence on the structure of Aβ plaques. Fibrillar Aβ plaques from 5XFAD mice at 4 mo of age were compact with well-defined, condensed cores and few surrounding diffuse structures (Fig. 3 F). In contrast, plaques from *Trem2*$^{-/-}$ 5XFAD mice appeared more loosely packed with smaller cores and many fiber-like structures extending outwards (Fig. 3 F). A quantitative morphology index based on the perimeter versus area of Aβ plaques in multiple brain sections confirmed TREM2-dependent differences in the morphology of Aβ plaques (Fig. 3 G). Furthermore, computation of pixels within Aβ plaque images demonstrated that plaque density was also TREM2 dependent (Fig. 3, H and I). Shape and density differences were also apparent in 8-mo-old mice (Fig. 3, F–I).

We sought to determine whether plaques from 5XFAD and *Trem2*$^{-/-}$ 5XFAD mice also differed in the biochemical profile of the Aβ deposits. It has been previously observed that Aβ plaques contain several Aβ subspecies resulting from truncation and/or posttranslational modification of the $A\beta_{1\text{-}42}$ peptides (DeMattos et al., 2012; Kummer and Heneka, 2014), including $A\beta_{p3\text{-}42}$, a truncated form of Aβ with a pyroglutamate modification at position 3 (Harigaya et al., 2000). To determine if the accumulation of Aβ subspecies was affected by TREM2 deficiency, we analyzed the insoluble fractions of Aβ from the brains of 8-mo-old 5XFAD, *Trem2*$^{+/-}$ 5XFAD, and *Trem2*$^{-/-}$ 5XFAD mice by denaturing acid/urea PAGE, followed by immunoblotting using antibodies against various epitopes of Aβ (DeMattos et al., 2002). We observed that the abundance of $A\beta_{p3\text{-}42}$ relative to $A\beta_{1\text{-}42}$ was reduced in the hippocampi of *Trem2*$^{+/-}$ 5XFAD and *Trem2*$^{-/-}$ 5XFAD mice. In addition, the relative abundance of other Aβ subspecies, such as $A\beta_{1\text{-}42\text{-}1}$ and $A\beta_{1\text{-}42\text{-}2}$, was reduced in a similar fashion in *Trem2*$^{+/-}$ 5XFAD and *Trem2*$^{-/-}$ 5XFAD mice (Fig. 3, J and K). Thus, TREM2 deficiency not only influences the physical appearance of the plaques, but also alters the Aβ subspecies composition.

TREM2 expression is important in limiting neuronal toxicity during the early stages of Aβ deposition

Because large, swollen, dystrophic axons and dendrites (neurites) are associated with Aβ plaques in AD and in mouse models with Aβ deposition (Masliah et al., 1996; Brendza et al., 2003), we examined whether altered plaque morphology and composition was also associated with increased neuronal damage. We stained sections for the N terminus (NT) of APP (NT-APP), which accumulates in dystrophic neurites, and measured NT-APP^{+} neuronal processes within 30 µm of Aβ plaques. We found that the number of dystrophic neurites was significantly increased in *Trem2*$^{-/-}$ 5XFAD mice compared with 5XFAD mice (Fig. 4, A–C). We also stained sections for hyperphosphorylated tau and found an increase in the number and volume of hyperphosphorylated tau punctae in *Trem2*$^{-/-}$ 5XFAD mice compared with 5XFAD mice (Fig. 4, D–E). Thus, the altered Aβ plaque shape and density associated with TREM2 deficiency observed in Fig. 3 were associated with increased toxicity to neural processes. Overall, these data indicate that TREM2-mediated microglial response is crucial in compacting Aβ plaques and preventing damage to the adjacent axons and dendrites.

Concluding remarks

A previous study proposed that TREM2 is important for infiltration of blood-derived monocytes into the brain, which then mediate Aβ plaque-associated reactive microgliosis (Jay et al., 2015). This study was based on phenotypic characterization of microgliosis with monocytic- and microglia-specific markers, along with bone marrow grafts, which enable tracking of congenically marked peripheral monocytes that traffic into the brain. However, phenotypic markers of migroglia, such as low expression of CD45 and high expression of the P2Y(12) receptor, are altered upon microglial activation and therefore do not precisely discriminate microglia from monocytes (Butovsky et al., 2014). Moreover, whole-body irradiation before bone marrow grafts causes a blood–brain barrier (BBB) leakage, facilitating an influx of blood monocytes that may obscure the relative contribution of distinct myeloid cell types during Aβ accumulation (Mildner et al., 2011). As parabiosis models do not rely on methods that may compromise the BBB, they may be more reliable than bone marrow grafts for determining the origin of microglia. Our parabiosis experiments indicate that the contribution of peripheral blood monocytes to microgliosis in mouse models of Aβ accumulation with an unperturbed BBB is undetectable. Moreover, staining of brain section with Ki67 suggested that Aβ-associated microgliosis depends at least in part on the proliferation of brain-resident microglia. Consistent with the predominant impact of brain-resident microglia in the response to amyloid, two recent studies showed that in a transgenic mouse model of Aβ deposition in which microglia are depleted after intracranial injection of gangliocyclovir and replaced with infiltrating monocytes, the infiltrating cells co-localize with Aβ plaques only after a long period of time and are not efficient at clearing plaques (Prokop et al., 2015; Varvel et al., 2015).

Recently, microglia around Aβ plaques were shown to form a physical barrier that prevents outward plaque expansion and leads to compact plaque microregions with low $A\beta_{1\text{-}42}$ affinity (Condello et al., 2015). Areas not covered by

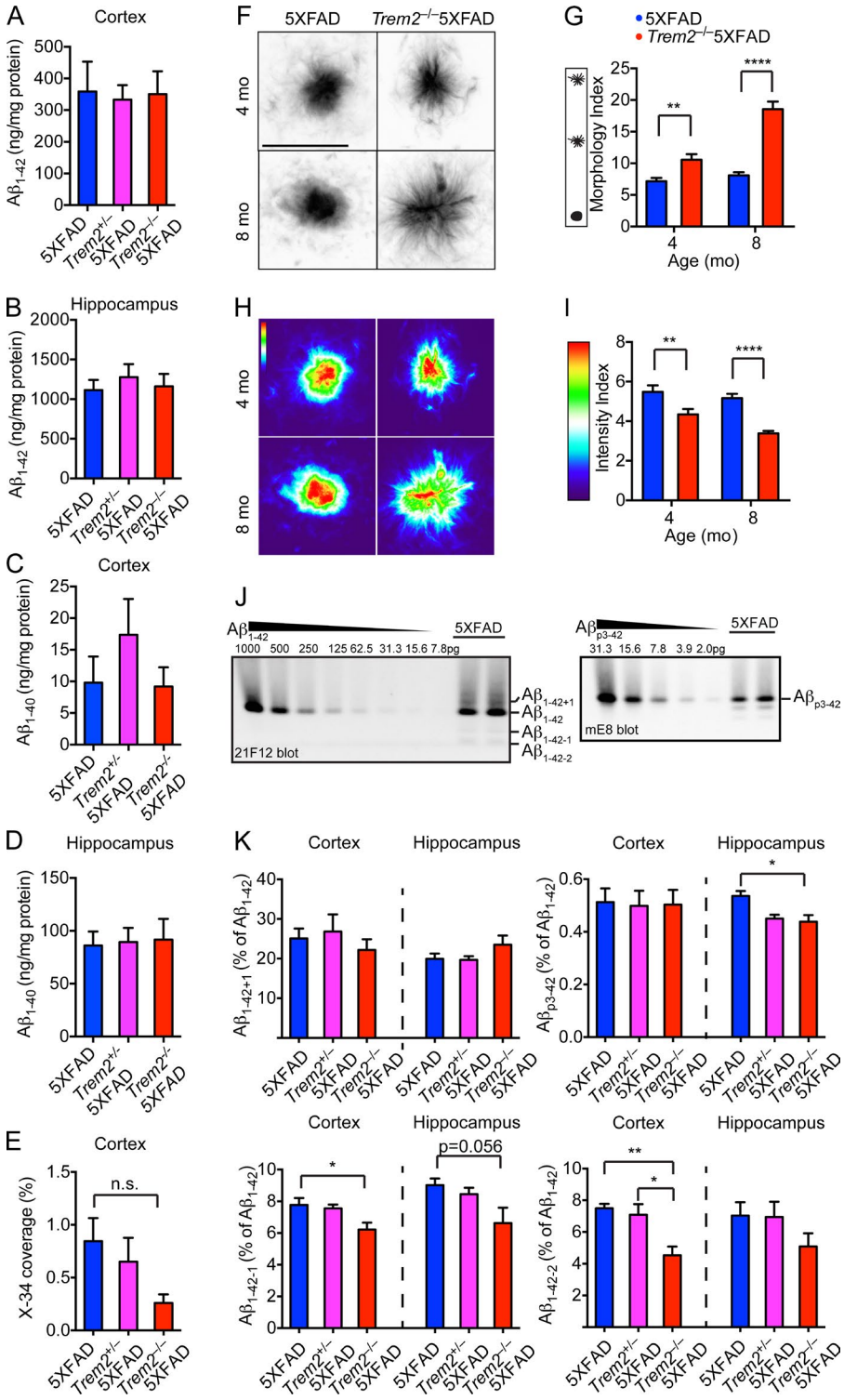

Figure 3. **TREM2 deficiency alters physical appearance and biochemical composition of amyloid plaques.** (A–D) Accumulation of insoluble $A\beta_{1-42}$ (A and B) and $A\beta_{1-40}$ (C and D) in the cortices and hippocampi of 4-mo-old 5XFAD, *Trem2*$^{+/-}$5XFAD, and *Trem2*$^{-/-}$5XFAD mice was determined by ELISA. (E) Deposition of fibrillar Aβ in the cortices determined by X-34 staining. Levels of X-34 signal in the hippocampi were below the threshold of detection. (F–I) Morphology of fibrillar plaques in 4-mo-old 5XFAD and *Trem2*$^{-/-}$*5XFAD* mice. X-34–reactive fibrillar plaques were visualized using high-resolution confocal microscopy (F) and converted to heat-map images based on pixel intensity (H). Physical appearance of X-34-reactive fibrillar plaques was further quantified based on morphology (G) and pixel intensity (I). Diffuse shape and reduced density were also apparent in 8-mo-old *Trem2*$^{-/-}$*5XFAD* mice (F and H). (J) Representative urea immunoblots showing the detection of $A\beta_{1-42}$, $A\beta_{1-42+1}$, $A\beta_{1-42-1}$, $A\beta_{1-42-2}$, and $A\beta_{p3-42}$ from insoluble fractions of hippocampi from 5XFAD mice. (K) Quantification of insoluble Aβ species by urea immunoblots in the cortices and hippocampi of 5XFAD, *Trem2*$^{+/-}$5XFAD, and *Trem2*$^{-/-}$5XFAD mice. Abundance of $A\beta_{1-42+1}$, $A\beta_{1-42-1}$, $A\beta_{1-42-2}$, and $A\beta_{p3-42}$ relative to $A\beta_{1-42}$ is shown. Amount of Aβ used for standard curves are indicated. Bar, 10 µm. *, $P < 0.05$; **, $P < 0.01$; ****, $P < 0.0001$, Mann-Whitney (G and I), two-way ANOVA (E and K). Data represent a total of 8–14 mice per group in A–E, eight mice per group in F–I and five mice per group in K. For confocal images, a total of four random HPF were analyzed per mouse. Error bar represents mean ± SEM.

microglia are less compact and contain protofibrillar hotspots with high $A\beta_{1-42}$ affinity, which are associated with more severe axonal dystrophy. Our data show that in the absence of TREM2-mediated microgliosis, Aβ plaques are less dense, more diffuse, and have some alterations in their biochemical features, exemplified by the reduced abundance of various Aβ subspecies in 5XFAD mice. Whether microglia influence the conversion of $A\beta_{1-42}$ into other Aβ species by enabling Aβ-modifying enzymes to act more efficiently on aggregated forms of Aβ remains an open question. More importantly,

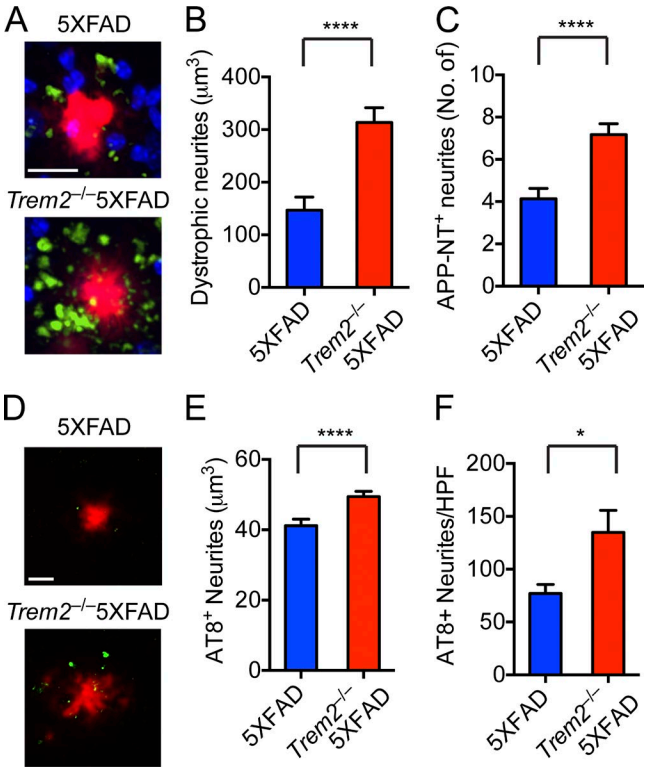

Figure 4. **Neuritic dystrophy and the amounts of phospho-tau in proximity to plaques are markedly increased in the absence of TREM2.** (A–C) Neuritic dystrophy in 5XFAD and *Trem2*$^{-/-}$5XFAD mice was visualized using 22C11 mAb against the APP N terminus (APP-NT). (A) Representative images show APP-NT^{+} neurites (green), Aβ plaques (X-34; red), and nuclei (To-pro3; blue). (B and C) Quantification of total volume and numbers of APP-NT^{+} neurites within 30 µm of Aβ plaques. (D–F) Hyperphosphorylated tau in 5XFAD and *Trem2*$^{-/-}$5XFAD mice. Sections were stained with anti–phospho-tau antibody (AT8; green) and Aβ plaques (red; D). Total volume of AT8^{+} neurites (E) and the number of AT8^{+} spots per HPF (F) were quantified. Bar, 20 µm. *, $P < 0.05$; ****, $P < 0.0001$, by Mann-Whitney. Data represent a total of four to eight mice per group. For confocal images, a total of four random HPF were analyzed per mouse. Error bar represents mean ± SEM.

the altered Aβ plaque morphology associated with TREM2 deficiency led to enhanced toxicity potential, as indicated by the increase in neuritic dystrophy. These results indicate that TREM2 has a major impact on the early containment of plaque diffusion by microglia. This impact is appreciable even at 4 mo of age, although the total Aβ present in TREM2-sufficient and -deficient 5XFAD mice is similar. We postulate that lack of this function for a long period of time leads to the increase in hippocampal $Aβ_{1-42}$ levels in 8-mo-old TREM2-deficient mice that we previously reported (Wang et al., 2015). Collectively, our studies highlight the protective role of TREM2 expression in brain-resident microglia by influencing the structure, biochemical composition, and toxicity of Aβ deposits and provide novel insights into the mechanisms by which TREM2 acts in the early stages of AD development.

MATERIALS AND METHODS

Mice. *Trem2*$^{-/-}$ mice were previously described (Turnbull et al., 2006). 5XFAD mice (Oakley et al., 2006) were purchased from The Jackson Laboratory (MMRRC) and crossed to *Trem2*$^{-/-}$ mice to generate *Trem2*$^{+/-}$5XFAD and *Trem2*$^{-/-}$5XFAD mice (Wang et al., 2015). Parabiotic mice were joined by the surgery core in the Hope Center for Neurological Disorders (Washington University, St. Louis, MO). In brief, the skin along the opposite flanks of parabiotic pairs was joined under general anesthesia and pairs were housed for the indicated postoperative time. All animal studies were approved by the Washington University Animal Studies Committee.

Preparation of brain samples. For histological analysis, mice were anesthetized with ketamine and perfused with ice-cold PBS. Right-brain hemispheres were fixed in 4% PFA overnight and placed in 30% sucrose before freezing and cutting on a freezing sliding microtome. Serial 40-µm coronal sections of the brain were collected from the rostral anterior commissure to caudal hippocampus as landmarks. For biochemical analysis, cortices, and hippocampi of the left-brain hemispheres were dissected out and flash frozen in liquid nitrogen.

Confocal imaging and quantification. 40-µm floating sections were stained with Iba-1 (Wako Pure Chemical Industries), X-34, and Topro-3 for visualization of microglia, plaques, and nuclei, respectively. Confocal images were collected using a Nikon A1R+ confocal microscope. 4–5 z-stack images (447 × 447 × 30 µm; 1.25 µm thickness) were acquired per animal in random cortical regions and hippocampal regions. Images were then processed with Imaris (Bitplane). Coordinates of microglia and the location and volume of Aβ plaques were identified using the Particle and Surface function, respectively, and imported into Matlab (Mathworks). Number of microglia within a 15- and 30-µm radius were then determined using an automated script. Dystrophic neurites were identified using 22C11 antibody against the N terminus of APP (EMD Millipore) followed by Alexa Fluor 555–conjugated anti–mouse IgG. Proliferating cells were identified using an anti–Ki-67-biotin (SolA15; eBioscience), followed by Alexa Fluor 488–conjugated streptavidin (Molecular Probes). Hyperphosphorylated tau was detected with AT8 antibody (Thermo Fisher Scientific). For plaque morphology analysis, high-resolution images were collected at 60× magnification with 1.5× digital zoom. Maximum intensity projection of the z-stack for each plaque was subsequently used for morphological analysis. To trace the shape of plaques, we applied a combination of intensity thresholds and edge detection in Matlab. First, the mean intensity of the brightest 10 pixels in the image (max intensity) was used to normalize the range. Pixels with intensity >0.5 times this max intensity formed a bright mask, and pixels <0.1 times this max formed a background mask. Next, edges were detected using the Laplacian of Gaussian method and dilated to generate a closed object. This object was overlaid with the bright mask, with the back-

ground mask used to eliminate edges that may appear in the background pixels. Finally, holes <50 pixels in the resulting plaque tracing were filled in, and the entire shape was smoothed out by image erosion with a diamond-shaped element to obtain the final shape. In summary, pixels brighter than 0.5 times max were included, pixels dimmer than 0.1 times max were excluded, and pixels between those values were determined by edge detection. The density index was defined as (no. perimeter pixels) × 4π/total no. of pixels; this increases with shape complexity, but is roughly size invariant. A perfect circle of any size would have a value near 1, and more complex shapes would have larger values.

The diffuseness of staining was also assessed using the z-projected plaque image. First, pixels <1% of max intensity were discarded as background pixels that were not part of the plaque. For this analysis, the shape tracing described above, which favors crisp edges, was not included so that more diffusely stained parts of the image could still be included in quantification. The cumulative intensity curve for the plaque image, starting with the brightest pixels and adding on progressively dimmer pixels, was compared with that of a "perfectly dense" curve, where all signal intensity is accounted for by maximum-intensity pixels. The area between these curves, normalized to the total intensity and the number of pixels, represents the deviation from a uniformly dense plaque. To obtain an index of density ranging from 0 to infinity, this area was inverted, and the lower limit of the resulting index, 2, was subtracted.

Denaturing acid/urea polyacrylamide gel electrophoresis (PAGE) and ELISA. A mouse anti–$A\beta_{33\text{-}42}$ antibody (21F12) was used for capture and biotinylated mouse anti–$A\beta_{1\text{-}5}$ antibody (3D6) or mouse anti–$A\beta_{p3\text{-}42}$ antibody (mE8) was used for detection of $A\beta_{1\text{-}42}$ or $A\beta_{p3\text{-}42}$, respectively (DeMattos et al., 2012), followed by streptavidin HRP (SouthernBiotech). All ELISAs were developed using Super Slow ELISA TMB (Sigma-Aldrich) and absorbance read on a Bio-Tek Epoch plate reader at 650 nm. The standard curves for each assay used synthetic human $A\beta_{1\text{-}42}$ or $A\beta_{p3\text{-}42}$ peptide (AnaSpec). Denaturing Acid/Urea PAGE was performed as previously described (DeMattos et al., 2002). Subsequent standard immunoblotting was used for Aβ identification.

In vivo phagocytosis assay for fibrillar Aβ. Mice were injected with methoxy-X04 (R&D Systems) at 10 mg/kg in a PBS/DMSO mixture at 1:1 ratio. Brains were isolated 3 h after injection and made into single-cell suspension as previously described (Heneka et al., 2013). Frequencies of methoxy-$X04^+$ microglia cells were determined by flow cytometry using a Canto II (BD) and analyzed using FlowJo (Tree Star).

Statistics. Data in figures are presented as mean ± SEM. All statistical analysis was performed using Prism (GraphPad Software). Statistical analysis to compare the mean values for multiple groups was performed using a one- or two-way ANOVA with correction for multiple comparisons. Comparison of two groups was performed using a two-tailed unpaired *t* test (Mann Whitney). Values were accepted as significant if $P \leq 0.05$.

ACKNOWLEDGMENTS

We thank the Hope Center Animal Surgery Core for performing parabiosis and Bakewell NeuroImaging Laboratory for help with confocal microscopy (Washington University School of Medicine). We thank J.D. Sedgewick and A.P. Martin (Eli Lilly and Company) for helpful suggestions and critical comments.

Y. Wang was supported by the Lilly Innovation Fellowship Award from Eli Lilly and Company. This work was funded by National Institutes of Health grants RF1 AG05148501 (M. Colonna), 5T32CA009547-30 (T.K. Ulland), and AG047644 (D.M. Holtzman), the National Multiple Sclerosis Society (grant RG4687A1/1; M. Cella), Cure Alzheimer's Fund (D.M. Holtzman and M. Colonna), the JPB Foundation (D.M. Holtzman), and the Knight Alzheimer's Disease Research Center pilot grant P50 AG005681-30.

Y. Wang, J.A. Tzaferis, J.T. Hole, and R.B. DeMattos are Eli Lilly and Company employees. The authors declare no additional competing financial interests.

Submitted: 14 December 2015
Accepted: 14 March 2016

REFERENCES

Brendza, R.P., C. O'Brien, K. Simmons, D.W. McKeel, K.R. Bales, S.M. Paul, J.W. Olney, J.R. Sanes, and D.M. Holtzman. 2003. PDAPP;YFP double transgenic mice: a tool to study amyloid-beta associated changes in axonal, dendritic, and synaptic structures. *J. Comp. Neurol.* 456:375–383. http://dx.doi.org/10.1002/cne.10536

Butovsky, O., M.P. Jedrychowski, C.S. Moore, R. Cialic, A.J. Lanser, G. Gabriely, T. Koeglsperger, B. Dake, P.M. Wu, C.E. Doykan, et al. 2014. Identification of a unique TGF-β-dependent molecular and functional signature in microglia. *Nat. Neurosci.* 17:131–143. http://dx.doi.org/10.1038/nn.3599

Cannon, J.P., M. O'Driscoll, and G.W. Litman. 2012. Specific lipid recognition is a general feature of CD300 and TREM molecules. *Immunogenetics.* 64:39–47. http://dx.doi.org/10.1007/s00251-011-0562-4

Condello, C., P. Yuan, A. Schain, and J. Grutzendler. 2015. Microglia constitute a barrier that prevents neurotoxic protofibrillar Aβ42 hotspots around plaques. *Nat. Commun.* 6:6176. http://dx.doi.org/10.1038/ncomms7176

Daws, M.R., P.M. Sullam, E.C. Niemi, T.T. Chen, N.K. Tchao, and W.E. Seaman. 2003. Pattern recognition by TREM-2: binding of anionic ligands. *J. Immunol.* 171:594–599. http://dx.doi.org/10.4049/jimmunol.171.2.594

DeMattos, R.B., M.A. O'dell, M. Parsadanian, J.W. Taylor, J.A. Harmony, K.R. Bales, S.M. Paul, B.J. Aronow, and D.M. Holtzman. 2002. Clusterin promotes amyloid plaque formation and is critical for neuritic toxicity in a mouse model of Alzheimer's disease. *Proc. Natl. Acad. Sci. USA.* 99:10843–10848. http://dx.doi.org/10.1073/pnas.162228299

DeMattos, R.B., J. Lu, Y. Tang, M.M. Racke, C.A. Delong, J.A. Tzaferis, J.T. Hole, B.M. Forster, P.C. McDonnell, F. Liu, et al. 2012. A plaque-specific antibody clears existing β-amyloid plaques in Alzheimer's disease mice. *Neuron.* 76:908–920. http://dx.doi.org/10.1016/j.neuron.2012.10.029

Gomez Perdiguero, E., C. Schulz, and F. Geissmann. 2013. Development and homeostasis of "resident" myeloid cells: the case of the microglia. *Glia.* 61:112–120. http://dx.doi.org/10.1002/glia.22393

Greter, M., and M. Merad. 2013. Regulation of microglia development and homeostasis. *Glia.* 61:121–127. http://dx.doi.org/10.1002/glia.22408

Guerreiro, R., and J. Hardy. 2014. Genetics of Alzheimer's disease. *Neurotherapeutics.* 11:732–737. http://dx.doi.org/10.1007/s13311-014-0295-9

Harigaya, Y., T.C. Saido, C.B. Eckman, C.M. Prada, M. Shoji, and S.G. Younkin. 2000. Amyloid beta protein starting pyroglutamate at position

3 is a major component of the amyloid deposits in the Alzheimer's disease brain. *Biochem. Biophys. Res. Commun.* 276:422–427. http://dx.doi.org/10.1006/bbrc.2000.3490

Heneka, M.T., M.P. Kummer, A. Stutz, A. Delekate, S. Schwartz, A. Vieira-Saecker, A. Griep, D. Axt, A. Remus, T.C. Tzeng, et al. 2013. NLRP3 is activated in Alzheimer's disease and contributes to pathology in APP/PS1 mice. *Nature.* 493:674–678. http://dx.doi.org/10.1038/nature11729

Holtzman, D.M., J.C. Morris, and A.M. Goate. 2011. Alzheimer's disease: the challenge of the second century. *Sci. Transl. Med.* 3:77sr1. http://dx.doi.org/10.1126/scitranslmed.3002369

Jay, T.R., C.M. Miller, P.J. Cheng, L.C. Graham, S. Bemiller, M.L. Broihier, G. Xu, D. Margevicius, J.C. Karlo, G.L. Sousa, et al. 2015. TREM2 deficiency eliminates TREM2+ inflammatory macrophages and ameliorates pathology in Alzheimer's disease mouse models. *J. Exp. Med.* 212:287–295. http://dx.doi.org/10.1084/jem.20142322

Karch, C.M., and A.M. Goate. 2015. Alzheimer's disease risk genes and mechanisms of disease pathogenesis. *Biol. Psychiatry.* 77:43–51. http://dx.doi.org/10.1016/j.biopsych.2014.05.006

Kummer, M.P., and M.T. Heneka. 2014. Truncated and modified amyloid-beta species. *Alzheimers Res. Ther.* 6:28. http://dx.doi.org/10.1186/alzrt258

Masliah, E., A. Sisk, M. Mallory, L. Mucke, D. Schenk, and D. Games. 1996. Comparison of neurodegenerative pathology in transgenic mice overexpressing V717F beta-amyloid precursor protein and Alzheimer's disease. *J. Neurosci.* 16:5795–5811.

Mildner, A., B. Schlevogt, K. Kierdorf, C. Böttcher, D. Erny, M.P. Kummer, M. Quinn, W. Brück, I. Bechmann, M.T. Heneka, et al. 2011. Distinct and non-redundant roles of microglia and myeloid subsets in mouse models of Alzheimer's disease. *J. Neurosci.* 31:11159–11171. http://dx.doi.org/10.1523/JNEUROSCI.6209-10.2011

Oakley, H., S.L. Cole, S. Logan, E. Maus, P. Shao, J. Craft, A. Guillozet-Bongaarts, M. Ohno, J. Disterhoft, L. Van Eldik, et al. 2006. Intraneuronal beta-amyloid aggregates, neurodegeneration, and neuron loss in transgenic mice with five familial Alzheimer's disease mutations: potential factors in amyloid plaque formation. *J. Neurosci.* 26:10129–10140. http://dx.doi.org/10.1523/JNEUROSCI.1202-06.2006

Otero, K., I.R. Turnbull, P.L. Poliani, W. Vermi, E. Cerutti, T. Aoshi, I. Tassi, T. Takai, S.L. Stanley, M. Miller, et al. 2009. Macrophage colony-stimulating factor induces the proliferation and survival of macrophages via a pathway involving DAP12 and beta-catenin. *Nat. Immunol.* 10:734–743. http://dx.doi.org/10.1038/ni.1744

Paloneva, J., T. Manninen, G. Christman, K. Hovanes, J. Mandelin, R. Adolfsson, M. Bianchin, T. Bird, R. Miranda, A. Salmaggi, et al. 2002. Mutations in two genes encoding different subunits of a receptor signaling complex result in an identical disease phenotype. *Am. J. Hum. Genet.* 71:656–662. http://dx.doi.org/10.1086/342259

Prinz, M., and J. Priller. 2014. Microglia and brain macrophages in the molecular age: from origin to neuropsychiatric disease. *Nat. Rev. Neurosci.* 15:300–312. http://dx.doi.org/10.1038/nrn3722

Prokop, S., K.R. Miller, N. Drost, S. Handrick, V. Mathur, J. Luo, A. Wegner, T. Wyss-Coray, and F.L. Heppner. 2015. Impact of peripheral myeloid cells on amyloid-β pathology in Alzheimer's disease-like mice. *J. Exp. Med.* 212:1811–1818. http://dx.doi.org/10.1084/jem.20150479

Takahashi, K., C.D. Rochford, and H. Neumann. 2005. Clearance of apoptotic neurons without inflammation by microglial triggering receptor expressed on myeloid cells-2. *J. Exp. Med.* 201:647–657. http://dx.doi.org/10.1084/jem.20041611

Tanzi, R.E. 2012. The genetics of Alzheimer disease. *Cold Spring Harb. Perspect. Med.* 2:10. http://dx.doi.org/10.1101/cshperspect.a006296

Tanzi, R.E. 2015. TREM2 and Risk of Alzheimer's Disease--Friend or Foe? *N. Engl. J. Med.* 372:2564–2565. http://dx.doi.org/10.1056/NEJMcibr1503954

Turnbull, I.R., S. Gilfillan, M. Cella, T. Aoshi, M. Miller, L. Piccio, M. Hernandez, and M. Colonna. 2006. Cutting edge: TREM-2 attenuates macrophage activation. *J. Immunol.* 177:3520–3524. http://dx.doi.org/10.4049/jimmunol.177.6.3520

Ulrich, J.D., M.B. Finn, Y. Wang, A. Shen, T.E. Mahan, H. Jiang, F.R. Stewart, L. Piccio, M. Colonna, and D.M. Holtzman. 2014. Altered microglial response to Aβ plaques in APPPS1-21 mice heterozygous for TREM2. *Mol. Neurodegener.* 9:20. http://dx.doi.org/10.1186/1750-1326-9-20

Varvel, N.H., S.A. Grathwohl, K. Degenhardt, C. Resch, A. Bosch, M. Jucker, and J.J. Neher. 2015. Replacement of brain-resident myeloid cells does not alter cerebral amyloid-β deposition in mouse models of Alzheimer's disease. *J. Exp. Med.* 212:1803–1809. http://dx.doi.org/10.1084/jem.20150478

Wang, Y., M. Cella, K. Mallinson, J.D. Ulrich, K.L. Young, M.L. Robinette, S. Gilfillan, G.M. Krishnan, S. Sudhakar, B.H. Zinselmeyer, et al. 2015. TREM2 lipid sensing sustains the microglial response in an Alzheimer's disease model. *Cell.* 160:1061–1071. http://dx.doi.org/10.1016/j.cell.2015.01.049